The IRM Quarterly
Fall 2004, Vol. 14, No. 3

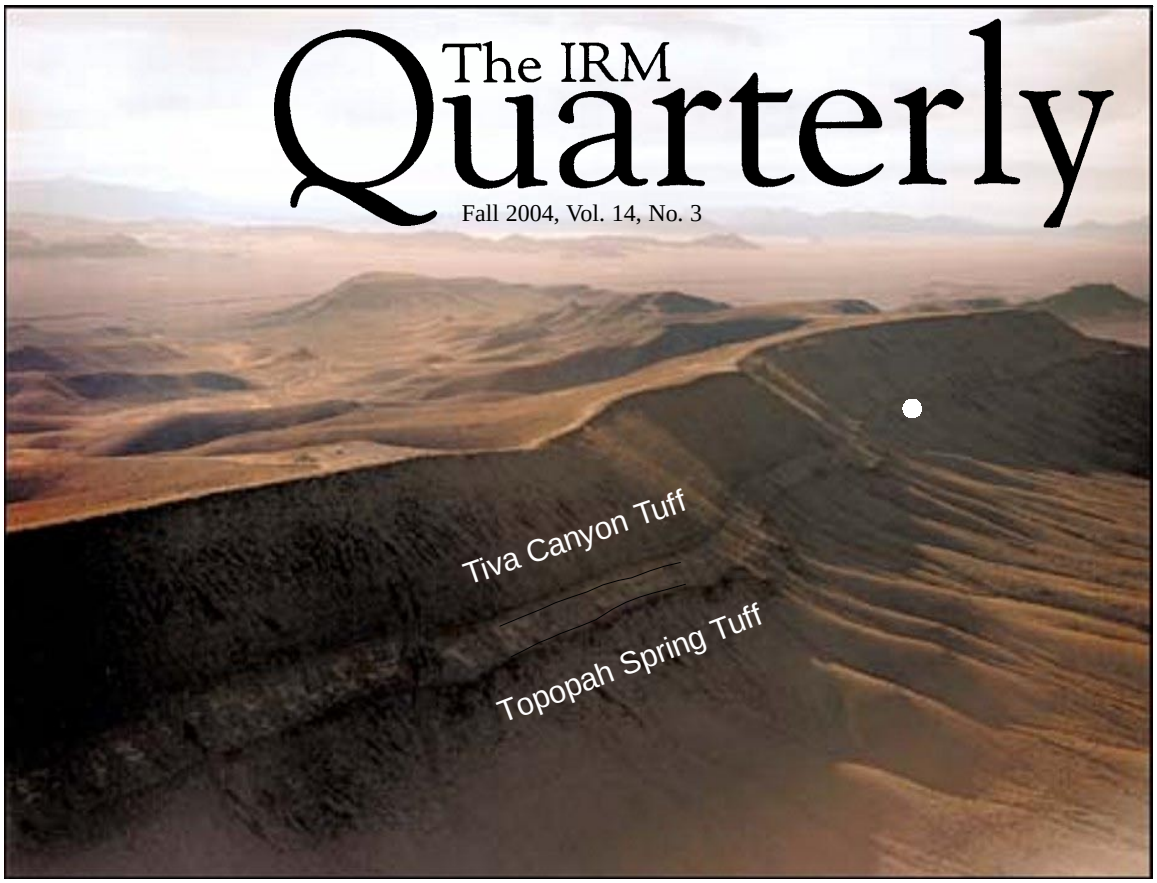

Aerial view of Yucca Mountain looking to the southeast. Unwelded tuffs, including the Yucca Mountain Tuff, separate two thick ash-flow sheets, the Tiva Canyon and Topopah Spring Tuffs. The dot shows the approximate location of the sampling site at the base of the Tiva Canyon.

Tiva Canyon Tuff (I)

Superparamagnetic Samples Available

Mike Jackson
Peat Sølheid
Brian Carter-Stiglitz
IRM
Joe Rosenbaum
USGS Denver
Jessica Till
Vassar College

As the proposed site for a national permanent nuclear waste repository, Yucca Mountain (in southern Nevada) has become one of the most intensely-studied locations on Earth (for a summary see http://www.ocrwm.doe.gov/documents/geology/index.htm). Spent fuel rods from nuclear power plants will continue to emit dangerous levels of radiation for hundreds of centuries, and the goal of the waste facility is to sequester this material securely for at least 10,000 years. The reasons for choosing this location for the repository are based on political geography, closed-basin hydrology and other factors, including the materials of which the mountain is composed: a series of silicic ash-flow and ash-fall tuffs.

Yucca Mountain is a long north-south trending ridge comprised largely of ash-flow tuffs of the Paintbrush Group. To the west lies Crater Flat; to the east are Jackass Flats, the repository Exploratory Studies Facility, the Nevada Test Site (where nuclear weapons tests were conducted between 1951 and 1992), and the notorious Area 51. To the north is the Timber Mountain caldera complex, the source of the Paintbrush Group (including the widespread Topopah Spring and Tiva Canyon Tuffs) and other voluminous Miocene tuffs. Tuffs have been proposed as a suitable material to entomb radioactive waste because of their favorable hydraulic properties and because in some layers they contain zeolites, which can absorb radionuclides.

Ash-flow tuffs have other interesting characteristics, including (to get to the point) their magnetic properties. Tuff samples from Yucca Mountain originally studied in the 1980's and 1990's [*Rosenbaum*, 1986, 1993; *Schlinger et al*., 1988, 1991] have been in more or less continuous circulation ever since, passed among aficionados like the legendary Dylan bootleg tapes. A compelling reason for the continuing interest in these particular samples [e.g., *Worm & Jackson*, 1999, 2000; *Pike et al 2001*; *Egli & Lowrie*, 2002] is their extraordinarily narrow distribution of magnetic grain sizes, combined with the uniform (unclustered) spatial distribution of magnetic particles, which minimizes their magnetostatic interactions.

Magnetic properties have a fantastic sensitivity to particle size (among other things), which is of central importance in paleomagnetism, rock magnetism, and environmental magnetism. The best way to understand this sensitivity is by studying samples like these tuffs, in which we have something that very closely approaches the theoretician's ideal assemblage of noninteracting identical grains. A great deal of effort has gone into producing synthetic materials with these characteristics (not only in rock magnetism, but in many fields of science and engineering). To date however, none (to our knowledge) has succeeded in achieving the combination of desirable features found in the Fe-Ti oxide assemblages in these tuffs.

Specifically, samples from the base of the Tiva Canyon Tuff contain Ti-poor titanomagnetites ($Fe_{3-x}Ti_xO_4$ with x~0.1, and minor Mn, Mg and Al), which crystallized and grew in volcanic glass at moderately high temperatures (~500-600°C) after emplacement of the flow. The grain size of these magnetites varies dramatically and systematically with stratigraphic position, from ~10 nm near the base and increasing systematically upward; within each horizon the particles are all nearly identical in size. Although questions remain about the precise mechanisms of growth, it seems clear that the size trend is generally related to the cooling history of the ash flow sheet.

tuffs

continued on p. 9...

Visiting Fellows' Reports

Stephanie Maes
University of Wisconsin-Madison
smaes@geology.wisc.edu

Separating complex magnetic anisotropies: Insizwa layered mafic complex, South Africa

The purpose of my multiple visits to the IRM was to address issues relating to the interpretation of magnetic fabrics within mafic-ultramafic rocks. We have been using HFAMS as a technique to document magmatic flow at the Insizwa layered mafic intrusion, South Africa. Samples for this study came from 3 vertical borehole cores, spaced 5 km apart. The advantage of using multiple boreholes is that we can examine changes in magnetic properties both as a function of depth as well as laterally.

While magnetic fabrics in felsic rocks have provided invaluable information on magmatic flow, magnetic fabrics in mafic-ultramafic rocks are significantly more difficult to interpret. Magnetic fabrics are complicated by the presence of multiple ferrimagnetic minerals [pyrrhotite and magnetite] as well as the occurrence of both multi-domain [MD] and single-domain [SD] magnetite grains. Because magnetite represents only a small volume in these rocks it is also important to document the fabric formed by mafic silicates.

I completed zero field heating and cooling experiments using the Quantum Designs Magnetic Properties Measurement System [MPMS] to determine the dominant magnetic carrier in 21 samples. The low temperature capabilities of the MPMS allow for the identification of magnetite and pyrrhotite based on low-temperature crystallographic transitions [e.g. Verwey transition in magnetite]. 10 of the 21 samples showed a strong Verwey transition at 120 K, which is associated with magnetite. Only 1 sample displayed the 34 K transition associated with pyrrhotite [Figure 1]. The remaining samples lack distinct transitions. Possible explanations for this are that the samples either contain no magnetite or magnetite has been sufficiently altered to suppress the Verwey transition. The lack of alteration of these samples, however, allows us to reject the latter explanation. Therefore, the magnetic data supports the conclusion that magnetite is the dominant ferrimagnetic mineral.

A series of hysteresis curves were acquired from a total of 166 cubes using the Vibrating Sample Magnetometer [VSM]. Saturation tests indicate that magnetite was saturated, therefore the HFAMS and calculated high field slope represent the orientation and magnetic susceptibility of mafic silicates [olivine and pyroxene]. Analysis of the hysteresis parameters also reveals a spatial pattern in domain size. In general PSD magnetite dominates but in the lower sill SD magnetite occurs [Figure 2]. This supports the conclusion of Ferré et al. [2002], who reported discrepancies between the AMS foliation and the mineral foliation, likely as a result of SD magnetite in the lower third of the Insizwa sill and from interstitially grown magnetite in the upper third.

I am currently working on techniques for measuring mineral fabric, such as image analysis of shape preferred orientation [SPO], which will yield a fabric that is independent of the magnetic fabric. Comparison of the SPO and AMS patterns will allow us to identify and examine any anomalous fabrics and the lithologies in which they exist.

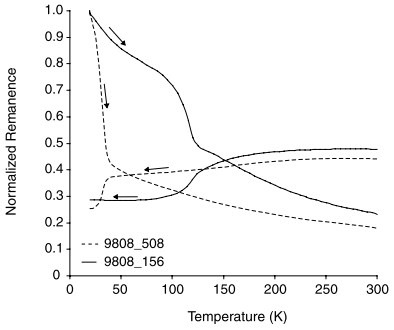

Figure 1. Remanence versus temperature heating and cooling curves illustrating the low temperature transitions in pyrrhotite (dashed line) and magnetite (solid line)

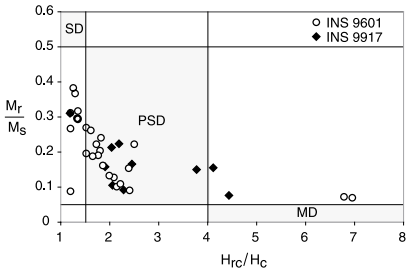

Figure 2. Day et al. (1977) plot of the hystersis parameters from borehole cores INS9601 and INS9917

Vincent Chevrier
Pierre-Etienne Mathé
CEREGE
chevrier@cerege.fr

Low Temperature Magnetic Properties Of Iron Bearing Minerals Weathered Under Simulated Martian Atmosphere

Introduction

The origin of iron bearing phases in the Martian regolith has been interpreted as the heritage of titanomagnetite present in the primary magmatic rocks as well as neoformed Fe^{3+} phases. However recent mass balance studies estimate that up to 10-30% in mass of the regolith matter could be of meteoritic origin, as meteorite and IDP usually contains 10-20 % of iron rich phases (sulfides and metal) compared to 1-2% in Martian rocks. Sulfides may also be more common in primary Martian rocks than on Earth. Moreover the use of natural terrestrial analogues does not acknowledge the fundamentally different nature of Earth and Mars atmosphere (replacement of O_2 by CO_2 and presence of peroxides) in terms of oxidation. Therefore various possible primary iron phases have been experimentally altered, including pure metallic iron, magnetite, as well as hexagonal and monoclinic pyrrhotites. Weathering was performed at room temperature and 0.8 bar in a pure CO_2 atmosphere, saturated either with water vapor or with hydrogen peroxide. The four experimentally weathered phases mentioned above have been characterized at different weathering steps, based on chemical analysis, X-ray, SEM, TEM, room and high temperature magnetic measurements.

Mineralogical Results

Results show that, while magnetite remains stable in both atmospheres, metal altered in water atmosphere is progressively converted into siderite ($FeCO_3$) which in turn transforms into goethite. Pyrrhotites react in both atmospheres, and are converted into mixture of sulfur, iron sulfates and (oxy)hydroxides. Iron sulfates may vary from Fe^{2+}-sulfates (melanterite) in water atmosphere to more complex assemblages of Fe^{3+}-sulfates (jarosite, coquimbite) in peroxide atmosphere. (Oxy)hydroxides are mainly goethite, but in some samples, lepidocrocite has also been found in comparable amounts to goethite. Most of these neoformed phases are nanosized requiring low temperature magnetic analyses down to liquid helium temperature.

Experiments Performed At The IRM

The characterization of low temperature magnetic behaviour of the samples has been carried out using MPMS FC-ZFC-RTSIRM procedure, Mössbauer, VSM and the Lakeshore for frequency dependance of the susceptibil-

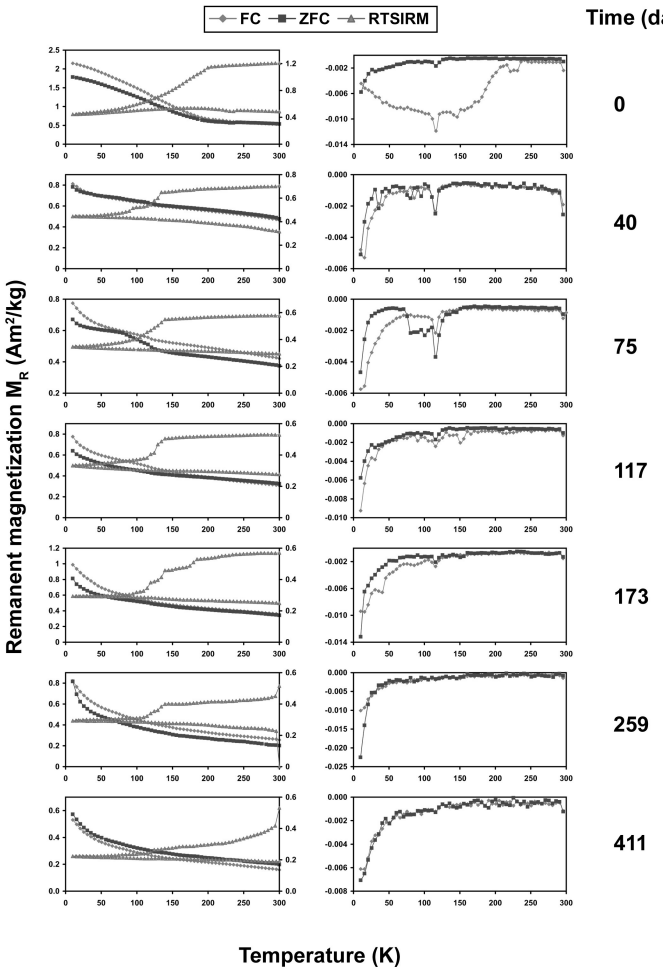

Figure 1 : FC-ZFC-RTSIRM curves of iron particles at different stages of weathering (left) and derivatives of FC-ZFC curve (right) showing the evolution of Verwey transition of neoformed magnetite.

ity. Due to the complexity of the mixture of iron and its neoformed products we will mainly focus on the results and preliminary interpretations obtained on this phase.

FC-ZFC curves of weathered iron metal evidence a Verwey transition at about 120 K, characterizing magnetite. This transition is particularly clear at 75 and 117 days of weathering, and progressively disappears after. However the very slight transition indicates that magnetite is only a trace in the neoformed products. Magnetite represents probably a metastable intermediate (Fe^{2+}, Fe^{3+}) phase during the transformation from siderite (Fe^{2+} phase) to goethite (Fe^{3+} phase). Its disappearance indicates either an oxidation into maghemite or goethite, either a diminution of grain size resulting from dissolution. RTSIRM curves of iron present very complex signal. Various transition temperatures appear only on cooling curve, whereas heating signal remains surprisingly flat. Some of these transitions occur at 120 K, indicating probable Verwey transition of neoformed magnetite, whereas others occur at 80 K, 140 K and 180 K. We have not found any clear relation between ageing time of iron and evolution of these transitions. We suppose that a part of these transitions result from interactions between iron particles, and between iron and neoformed magnetite. Other features may also indicate the presence of interactions in the mixture. Indeed the cooling branch of the RTSIRM curve progressively converges towards the flat heating curve. This convergence upon ageing indicates a diminution of the interactions between iron particles, or an evolution from harder to softer material. This may result from an increase of the distance between particles, due to two combined effects : the diminution of the size of iron particles and the thickness of layers of neoformed products on the surface of the grains. The presence of interactions may also be responsible for the absence of any dependance of susceptibility with frequency. Alternatively, some features may also be assigned to some “exotic” intermediate phases during alteration process.

Mössbauer spectra of iron give useful information on the phases present during weathering. Mössbauer spectra acquired at 75 days evidence the beginning of ordering of a phase at temperatures below 80 K. This temperature is higher than ordering temperature of siderite (around 35 K), and is only attributable to iron (oxy)hydroxides. X-ray analyses indicate that goethite is poorly crystalline, and that 2L-ferrihydrite like product is present in substantial amounts. Therefore the sextet appearing at 80 K may be related to a mixture between goethite and ferrihydrite, or to an intermediate phase during goethite condensation from ferrihydrite. This assumption is supported by the spectra taken at 411 days, showing a complete ordering of the goethite at 80 K. Alternatively, due to the broad sextet at 4.2 K in the spectrum obtained at 75 days, we do not exclude the possible contribution of siderite, which is ordered at this temperature.

Conclusions

Our magnetic measurements conducted at the IRM on weathering products in Martian conditions indicate the complexity of the signal generated for mixture of three dominating phases (iron, siderite, goethite). The observation of magnetite during weathering is of primary importance as providing a possible source for highly magnetic material observed by landers in the Martian regolith. The complexity of the signals observed on FC-ZFC-RTSIRM curves indicates that a great variety of phenomena occur during weathering, including variations of interactions between iron particles and possible neoformation of “exotic” metastable phases. We intend to better characterize these transitions using Mössbauer spectroscopy, high field induced magnetization at low temperature (detection of possible hematite) and by investigating divergences between FC-ZFC. We would like also to highlight that the apparent complexity observed in the signals of iron may be simplified in the case of more complex mixtures. Indeed, this apparent paradox may be simplified by the fact that dissolution of iron particles in a matrix (a meteorite or a regolith) may result in a strong diminution of the interactions supposed here.

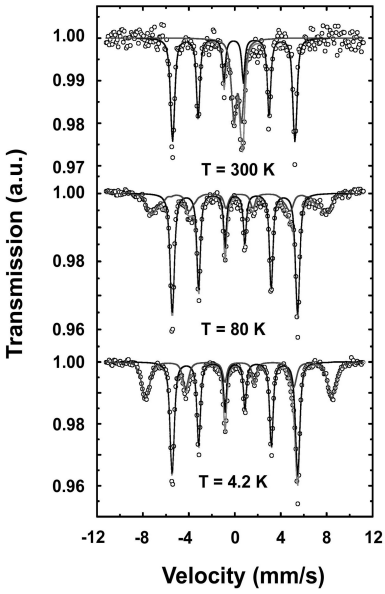

Figure 2 : Mössbauer spectra of iron particles at 75 days of weathering, obtained at different temperatures (300 K, 80 K and 4.2 K).

…VF Reports
continued from p. 3

Magnetic property variations of various ferrous and non-ferrous minerals treated in a microwave H-field

Dr. Ramesh Peelamedu (P.D.Ramesh)
Materials Research Institute
The Pennsylvania State University
pdramesh@psu.edu

Microwaves are high frequency electromagnetic waves widely used for materials processing. Unlike in a conventional heating element furnace, materials processed in a microwave cavity are exposed to thermal and non-thermal radiations during processing. However, on many occasions, these effects are highly indistinguishable, lie in each other's pocket and become really difficult to isolate the individual contributions. This issue has been partially resolved by use of a single mode cavity with E (electric) and H (magnetic) field active regions, wherein, it is possible to isolate the E-field maximum and H-field maximum regions. Experiments on the H-field treatment of various magnetic materials have yielded astonishing results[1, 2]. Magnetic compounds decrystallize, undergo structural and microstructural changes (psuedo-amorphic), and undergo serious magnetic property changes. This effect is quite new and discovered for the first time by Roy and co-workers in various ceramics materials at the Pennsylvania State University. *IRM* awarded my proposal to carry out measurement of magnetic properties of several minerals treated in microwave H field cavity.

Sixteen different natural minerals were treated for various durations up to a maximum of 180s in a H-field cavity. The chosen minerals and the treatment schedules are given in table 1.

Both untreated and H-field treated minerals were characterized using a Princeton Measurements Vibrating Sample Magnetometer at the *IRM*. Each M-H measurement was averaged out for 4-5 pieces obtained from different parts of each mineral sample. Despite the fact that most of the minerals in the table contain Fe ions, the strongest H-field interaction was observed in samples that had a partial ferro/ferri magnetic behavior. Samples that are highly paramagnetic, showed either a very minute change or no change at all. Figure 1 shows the M-H curves obtained for untreated and treated Lodestone samples.

All the H-field decrystallized minerals show a noticeable change in the M-H curve characteristics. The magnetization value increases by 20 –30% and coercive field (Hc) tend to become zero. The enlarged version of Figure 1 is shown as Figure 2, clearly show a decrease in coercive field value from 142 Oe to 48 Oe.

Similar results have been observed for Magnetite, Ilmenite, and Hematite minerals. The untreated Pyrite and Arsenopyrite minerals show a paramagnetic M-H behavior but H-field treatment of these minerals for 30 seconds or less has created some ferromagnetic species (Figure 3). Since all the field treatment experiments were carried out in air, it is quite possible that these minerals could have oxidized partially. A similar behavior was noticed for Pyrohotite mineral also. On the other hand, M-H curve of Pyroluscite mineral hardly show any change after H-field treatment.

Minerals namely Goethite, Chromite, Franklinite and Mica failed to exhibit any variation in the M-H graph even after 90 s H-field treatment. Presently, I am involved in correlating the magnetic properties to crystal structure and microstructure.

Following are the conclusions of this work:

(i) Ferromagnetic minerals interact strongly with the microwave H-field. Some minerals decrystallize, create a mayhem in the lattice structure, and exhibit colossal variation in magnetic properties.

(ii) It can be generalized that the M-H curve of decrystallized mineral exhibit an increase in magnetization value and decrease in coercivity compared to the untreated ones.

References:

1. R. Roy, R. Peelamedu, L. Hurtt, J.Cheng, D.Agrawal, Definitive experimental evidence for microwave effects: radically new effects of separated E and H fields, such as decrystallization of oxides in seconds, *Materials Research Innovations* (2002), 6(3), 128-140.
2. R.Roy, R. Peelamedu, C.A. Grimes, J.Cheng, D. Agrawal, Major phase transformations and magnetic property changes caused by electromagnetic fields at microwave frequencies. *Journal of Materials Research* (2002), 17(12), 3008-3011.

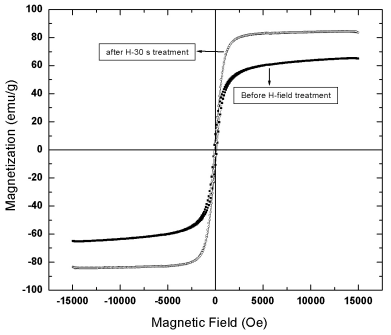

Figure 1 : *Room temperature M-H curves measured for H-field treated and untreated Lodestone samples*

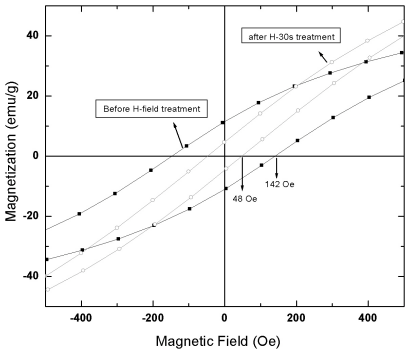

Figure 2: *Decrease in coercive field values observed after H-field treatment in Lodestone samples*

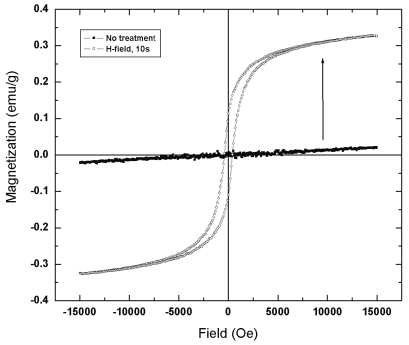

Figure 3: *Room temperature M-H curves measured for H-field treated and untreated Arsenopyrite samples*

Composition	Time (seconds)	Atmosphere	Heating Performance
Arsenopyrite	10, 30 (90% power)	Air	None
Arsenopyrite	30	Argon	Moderate
Arsenopyrite (transparent)	15	Air	None
Chromite	30, 60, 180	Air	None, Low
Franklinite	30, 60	Air	None
Goethite	30, 60, 120	Air	None
Hematite	30, 60	Air	Moderate-High
Ilmenite	30, 60, 180	Air	Moderate-High
Lodestone	30, 60	Air	Moderate-High
Magnetite	30, 60, 180	Air	Moderate - High
Mica-Biotite	30, 60, 180	Air	None
Pyrite	5 (80%), 120 (80%)	Air	Shattered
Pyrohotite	30, 60, 180	Air	Moderate
Pyrolusite	30, 60	Air	Low
Spinel Ceylon	30, 60	Air	None
Tourmaline	30, 60, 180	Air	Low

THE

LONDON, EDINBURGH, AND DUBLIN

PHILOSOPHICAL MAGAZINE

AND

JOURNAL OF SCIENCE.

[FIFTH SERIES.]

APRIL 1896.

XXXI. *On the Influence of Carbonic Acid in the Air upon the Temperature of the Ground.* *By* Prof. SVANTE ARRHENIUS *.

I. *Introduction : Observations of* Langley *on Atmospherical Absorption.*

A GREAT deal has been written on the influence of the absorption of the atmosphere upon the climate. Tyndall † in particular has pointed out the enormous importance of this question. To him it was chiefly the diurnal and annual variations of the temperature that were lessened by this circumstance. Another side of the question, that has long attracted the attention of physicists, is this : Is the mean temperature of the ground in any way influenced by the presence of heat-absorbing gases in the atmosphere ? Fourier‡ maintained that the atmosphere acts like the glass of a hot-house, because it lets through the light rays of the sun but retains the dark rays from the ground. This idea was elaborated by Pouillet § ; and Langley was by some of his researches led to the view, that " the temperature of the earth under direct sunshine, even though our atmosphere were present as now, would probably fall to −200° C., if that atmosphere did not possess the quality of selective

* Extract from a paper presented to the Royal Swedish Academy of Sciences, 11th December, 1895. Communicated by the Author.
† 'Heat a Mode of Motion,' 2nd ed. p. 405 (Lond., 1865).
‡ *Mém. de l'Ac. R. d. Sci. de l'Inst. de France*, t. vii. 1827.
§ *Comptes rendus*, t. vii. p. 41 (1838).

Current Abstracts

A list of current research articles dealing with various topics in the physics and chemistry of magnetism is a regular feature of the IRM Quarterly. *Articles published in familiar geology and geophysics journals are included; special emphasis is given to current articles from physics, chemistry, and materials-science journals. Most abstracts are culled from* INSPEC *(© Institution of Electrical Engineers),* Geophysical Abstracts in Press *(© American Geophysical Union), and* The Earth and Planetary Express *(© Elsevier Science Publishers, B.V.), after which they are subjected to Procrustean editing and condensation for this newsletter. An extensive reference list of articles (primarily about rock magnetism, the physics and chemistry of magnetism, and some paleomagnetism) is continually updated at the* IRM. *This list, with more than 5200 references, is available free of charge. Your contributions both to the list and to the Abstracts section of the* IRM Quarterly *are always welcome.*

Environmental Magnetism and Paleoclimate Proxies

Egli, R., 2004, **Characterization of individual rock magnetic components by analysis of remanence curves. 3. Bacterial magnetite and natural processes in lakes**: *Physics & Chemistry of the Earth, v.29,* no.13-14, p.869-884.
The simplification of the unmixing problem proposed in this paper is based on an iterative linearization procedure, which considers the variability of magnetic components. A combination of four parameters, so-called magnetic fingerprints, is sufficient for a complete characterization of the remanent magnetization of a component. These magnetic fingerprints are used in tracking the response of Baldeggersee (Switzerland) to environmental changes, with special regard to the role of bacterial magnetite in the iron cycle and its possible use as a sensitive paleoredox indicator.

Geiss, C. E., Banerjee, S. K., Camill, P. and Umbanhowar, C. E., 2004, **Sediment-magnetic signature of land-use and drought as recorded in lake sediment from south-central Minnesota, USA**: *Quaternary Research, v.62,* no.2, p.117-125.
The onset of European-style farming led to increased erosion, reflected in high values of κ, IRM and ARM. Recent sediment also contains authigenic SD magnetite, most likely from magnetotactic bacteria. A comparison with older Holocene sediment from the same lake shows that, over time, most of the fine magnetic signal is lost after deposition, leading to decreases in magnetization and a bimodal grain size distribution of SP and MD particles, evident from ARM/IRM ratios, hysteresis, and low-temperature analyses.

Grimley, D. A., Arruda, N. K. and Bramstedt, M. W., 2004, **Using magnetic susceptibility to facilitate more rapid, reproducible and precise delineation of hydric soils in the midwestern USA**: *Catena, v.58,* no.2, p.183-213.
At five sites in Illinois with contrasting soil types and glacial histories, the κ values of surface soils were consistently higher in well-drained soils and lower in hydric soils, reflecting anaerobic deterioration of both detrital magnetite and soil-formed ferrimagnets. SEM images display significantly more detrital magnetite alteration in hydric soils. Fly ash typically accounts for 5-15% of the total κ, and fly ash particles are also more altered in low κ soils, implying that significant magnetite dissolution can occur in < 150 years.

Lagroix, F. and Banerjee, S. K., 2004, **The regional and temporal significance of primary aeolian magnetic fabrics preserved in Alaskan loess**: *Earth & Planetary Science Letters, v.225,* no.3-4, p.379-395.
The temporal variations of inferred paleowind directions track paleoclimatic glacial-interglacial cycles, and provide additional constraints to the geochronology of the loess deposit. The overall average paleowind directions at two sites are similar, confirming a regional (spatial) consistency of past surface air circulation.

Reitz, A., *et al.*, 2004, **A combined geochemical and rock-magnetic investigation of a redox horizon at the last glacial/interglacial transition**: *Physics & Chemistry of the Earth, v.29,* no.13-14, p.921-931.
Redox boundaries moved down into the sediment at the last glacial/interglacial transition and subsequently upwards during the Holocene, producing conspicuous double peaks for Fe and Mn. The geochemical reconstruction is supported by χ and magnetization measurements displaying well-defined anomalies in the vicinity of active and paleo redox boundaries. Moreover, the small scale movement of the Fe^{2+}/Fe^{3+} redox-boundary could be traced in detail by overlaying the peak-shape pattern of V/A1 and of χ_f/χ_{tot}.

Salome, A. and Meynadier, L., 2004, **Magnetic properties of rivers sands and rocks from Martinique Island: tracers of weathering?**: *Physics & Chemistry of the Earth, v.29,* no.13-14, p.933-945.
Sands were sampled in several riverbeds on the island while rocks were taken in the surrounding lava flows. Hysteresis loops and χ(T) are similar for parent rocks and their weathering products. Small differences are detectable due to weathering, but this does not affect the magnetic parameters enough to induce problems in their use as tracers of magnetic sources.

Sangode, S. J. and Bloemendal, J., 2004, **Pedogenic transformation of magnetic minerals in Pliocene-Pleistocene palaeosols of the Siwalik group, NW Himalaya, India**: *Palaeogeography Palaeoclimatology Palaeoecology, v.212,* no.1-2, p.95-118.
Rock magnetic and geochemical analyses indicate a predominance of hematite and goethite. The relative contributions of goethite and hematite are derived from differential rates of IRM acquisition, which are further confirmed using stepwise thermal demagnetisation of orthogonal IRM components acquired at 4, 1 and 0.3 T. The earliest Pliocene palaeosol shows pedogenic depletion of χ due to the transformation of parental ferrimagnetic minerals mainly into anti ferromagnetic minerals; in the youngest (middle Pleistocene) profile the reverse transformation is evident.

Vlag, P. A., Kruiver, P. P. and Dekkers, M. J., 2004, **Evaluating climate change by multivariate statistical techniques on magnetic and chemical properties of marine sediments (Azores region)**: *Palaeogeography Palaeoclimatology Palaeoecology, v.212,* no.1-2, p.23-44.
Variations in magnetic mineral concentration and Ti/Al ratios can be linked to detrital input and coincide with $\delta^{18}O$ changes. The highest concentrations are found around temperate periods, when detrital input from the Azores Islands is most prominent. Lower Ti/Al ratios and a slightly different composition of the lithogenic fraction suggests the presence of a second, probably eolian, detrital component during glacial periods.

Magnetic Field Records and Paleointensity Methods

Carvallo, C., Ozdemir, O. and Dunlop, D. J., 2004, **Palaeointensity determinations, palaeodirections and magnetic properties of basalts from the Emperor seamounts**: *Geophysical Journal International, v.156*, no.1, p.29-38.
According to the selection criteria traditionally used in palaeointensity determination, 17 samples give a reliable result. The samples show a very wide variety in unblocking temperatures, due to variation in titanium content and the oxidation state of titanomagnetites. Thermomagnetic curves enabled us to identify titanomaghemite in several lava flows. After rejecting the results from samples showing evidence of maghemitization, only four samples can be considered as truly reliable, with values between 34.2 and 36.9 μT.

Leonhardt, R., Krasa, D. and Coe, R. S., 2004, **Multidomain behavior during Thellier paleointensity experiments: a phenomenological model**: *Physics of the Earth & Planetary Interiors, v.147*, no.2-3, p.127-140.
pTRM*-tails significantly affect the shape of the Arai diagram. Concave curvature of the Arai plot for samples containing MD particles is related to remanences with $T_{ub}<T_b$. pTRM*-tails, however, which affect T_{ub}s above the respective T_bs, lead to a convex shape. An overlap of both convex and concave characteristics can produce s-shaped Arai diagrams. The effect of pTRM*-tails is strongly dependent on the angle and intensity difference between applied field and NRM of the sample. A new method for calculation of the pTRM*-tail check is proposed which accounts for such angular difference, as well as intensity differences. Conducting the Thellier experiment with alteration checks, pTRM*-tail checks, and additivity checks at an angle between NRM and laboratory field > 0, provides the possibility to unequivocally identify multidomain bias.

McArdle, N. J., Halls, H. C. and Shaw, J., 2004, **Rock magnetic studies and a comparison between microwave and Thellier palaeointensities for Canadian Precambrian dykes**: *Physics of the Earth & Planetary Interiors, v.147*, no.2-3, p.247-254.
Thermomagnetic analyses show a single distinct T_C at 585°C indicating pure magnetite. Hysteresis and backfield IRM measurements suggest grains within the PSD size range. Lowrie-Fuller tests suggest that single domain grains carry the remanence. High quality palaeointensity estimates were obtained, showing markedly low palaeointensities throughout the Proterozoic, VDMs typically being less than 4×10^{22} Am^2, less than half the value of the present field.

Mochizuki, N., *et al.*, 2004, **Palaeointensity study of the Oshima 1986 lava in Japan: implications for the reliability of the Thellier and LTD-DHT Shaw methods**: *Physics of the Earth & Planetary Interiors, v.146*, no.3-4, p.395-416.
The palaeointensities determined by Coe's version of the Thellier method ranged are systematically higher than the expected intensity, with a relation to the high-temperature oxidation state. Directional changes of NRM during the Thellier experiments indicate that most of the samples acquired CRM due to laboratory heating as some magnetic phase with high T_b was produced. We also applied the double heating technique of the Shaw method combined with LTD; the average agrees with the expected intensity indicating no dependence on the high-temperature oxidation states.

Magnetic Microscopy and Spectroscopy

Frandsen, C., *et al.*, 2004, **Magnetic domain structures and stray fields of individual elongated magnetite grains revealed by magnetic force microscopy (MFM)**: *Physics of the Earth and Planetary Interiors, v.141*, no.2, p.121-9.
In a sample with an intense NRM, a norite from Heskestad, Norway, we used MFM to study seven magnetite exsolution lamellae, of which five were about 30 μm long and a few micrometers wide, and two were significantly shorter; all were located in their natural host, a grain of clinopyroxene. By combining MFM images with shape information, the internal domain structure was determined for individual grains. In general, the lamellae were PSD with open-flux domain magnetisations parallel to their long axes. The domain sizes were, in cross-section, on the order of a micrometer for the longer lamellae and about 300 nm for the short lamellae.

Gao, L., *et al.*, 2004, **Focused ion beam milled CoPt magnetic force microscopy tips for high resolution domain images**: *IEEE Transactions on Magnetics, v.40*, no.4 Part 2, p.2194-2196.
High-coereivity CoPt MFM tips have been modified by focused ion beam milling to improve the resolution of magnetic domain images. The magnetic materials around the apex have been removed, leaving a 30-nm diameter magnetic particle at the tip end. Due to the smaller amount of magnetic material, the stray field from this new tip is significantly reduced, and the spatial resolution of the magnetic domain images is improved to ~ 11 nm under ambient conditions with a commercial magnetic force microscope.

Helgason, O., 2004, **Processes in geophysics studied by Mossbauer spectroscopy**: *Hyperfine Interactions, v.156*, no.1, p.379-388.
Mossbauer spectroscopy has been appreciated in geoscience as a powerful tool to study magnetic and structural properties of a wide range of minerals and rocks. In this presentation the application of Mossbauer spectroscopy in different geophysical processes such as tracing the development of magma during volcanic eruptions and phase transitions of magnetic minerals due to thermal impact of dikes in earlier lava formation or hydrothermal alteration will be discussed.

Lo, C. C. H., Paulsen, J. A., Kinser, E. R. and Jiles, D. C., 2004, **Quantitative evalutation of stress distribution in magnetic materials by Barkhausen Effect and magnetic hysteresis measurements**: *IEEE Transactions on Magnetics, v.40*, no.4 Part 2, p.2173-2175.
Using a newly developed magnetic imaging system, magnetic measurements can be usefully used for detecting stress concentration in magnetic materials nondestructively. The system measured hysteresis loop and Barkhausen effect signal using a surface sensor, and converted the data into a two-dimensional image showing spatial variations in magnetic properties. When compressive stresses were applied along the neutral axis of the sample, the image of magnetic properties such as coercivity exhibited patterns which were similar to the stress distributions calculated using finite element model (FEM).

Szymanski, K., Satula, D. and Dobrzynski, L., 2004, **Angular distribution of hyperfine magnetic field in Fe3O4 and Fe66Ni34 from Mossbauer polarimetry**: *Hyperfine Interactions, v.156*, no.1, p.21-26.
Experimental determination of some angular averages of hyperfine field is demonstrated. The averages relates to magnetic structure. Exemplary results of the measurements for Fe3O4 and Fe66Ni34 show that it is possible to obtain valuable information about the field magnitudes and orientations even when distributions of fields are present in the system under study. [References: 16]

Williams, A. G. B. and Scherer, M. M., 2004, **Spectroscopic evidence for Fe(II)-Fe(III) electron transfer at the iron oxide-water interface**: *Environmental Science & Technology, v.38*, no.18, p.4782-4790.
Using the isotope specificity of ^{57}Fe Mossbauer spectroscopy, we report observations of Fe(II) reacted with oxide surfaces under conditions typical of natural environments (i.e., wet, anoxic, ~neutral pH, and ~ 1% Fe(II)). Mossbauer spectra of Fe(II) adsorbed to rutile (TiO_2) and aluminum oxide (Al_2O_3) show only Fe(II) species, whereas spectra of Fe(II) reacted with goethite (α-FeOOH), hematite (α-Fe_2O_3), and ferrihydrite (Fe_5HO_8) demonstrate electron transfer between the adsorbed Fe(II) and the underlying iron(III) oxide.

Magnetization & Demagnetization Processes

Fabian, K. and Shcherbakov, V. P., 2004, **Domain state stabilization by iterated thermal magnetization processes**: *Geophysical Journal International, v.159*, no.2, p.486-494.
According to fundamental assumptions a remanence acquired at some temperature T is not influenced by subsequent heating and cooling cycles. This is tested for natural and synthetic multidomain particle ensembles in the case of the tail of pTRM. The experimental results for all samples show that repeating the acquisition process for the tail leads to an asymptotic saturation and can be explained in terms of a statistical theory. Iterative saturation of the tail of pTRM can be interpreted using a combination of exponential saturation functions related to the subspectrum of the involved transition matrix.

Kletetschka, G., *et al.*, 2004, **An empirical scaling law for acquisition of thermoremanent magnetization**: *Earth & Planetary Science Letters, v.226*, no.3-4, p.521-528.
The remanence efficiency $\varepsilon(T_r)$ is the ratio of the $M_{tr}(T_r)$ to $J_{sr}(T_r)$. We report a power law

relationship with exponent related to $J_s(T_r)$ and unit slope indicating a linear relationship between the acquisition magnetic field, B, and $M_{tr}(T_r)$ measured at room temperature T_r. Thus $\log(\varepsilon(T_r))$ of $M_{tr}(T_r)$ in magnetic minerals of contrasting $J_s(T_r)$ plots linearly with log(B) along separate grain-size-independent straight lines with nearly unit slope and offsets related to $J_s(T_r)$, This empirical relationship predicts strong magnetization of hematite and pyrrhotite in weak fields, and can be used as an assessment tool for observed remanence in planetary and meteoritic objects.

McClelland, E., Wilson, C. J. N. and Bardot, L., 2004, **Palaeotemperature determinations for the 1.8-ka Taupo ignimbrite, New Zealand, and implications for the emplacement history of a high-velocity pyroclastic flow**: *Bulletin of Volcanology, v.66*, no.6, p.492-513.
Equilibrium temperatures from sites less than 30-40 km from vent are 150-300 °C, whereas at greater distances site equilibrium temperatures increase up to 400-500 °C. The similar, but offset, increases in equilibrium temperatures for medial and distal layers 1 and 2 are consistent with both layers being deposited from the same flow. These data support previous interpretations that a concentrated basal flow played a dominant role in emplacement and deposition of the Taupo ignimbrite.

Roshko, R. M. and Viddal, C., 2004, **Interpreting remanence isotherms: a Preisach-based study**: *European Physical Journal B, v.40*, no.2, p.145-151.
Numerical simulations of the field dependence of the isothermal remanent moment (IRM) and the thermoremanent moment (TRM) are presented, based on Preisach formalization. They show that the TRM saturates more rapidly than the corresponding IRM. IRM is determined primarily by the distribution of dissipation fields and TRM by the mean dissipation field and the dispersion of bias fields. A regime where the TRM and the IRM provide independent scans of the Preisach distribution is identified. These systematics are exploited to analyze data.

Saitoh, E., Miyajima, H., Yamaoka, T. and Tatara, G., 2004, **Current-induced resonance and mass determination of a single magnetic domain wall**: *Nature, v.432*, no.7014, p.203-206.
The DW mass sets the ultimate operation speed of these devices, but has yet to be determined experimentally. We report the direct observation of the dynamics of a single DW in a ferromagnetic nanowire, which demonstrates that the wall has a very small but finite mass of 6.6×10^{-23} kg. We prepared a tunable DW potential in the nanowire, and detected its resonance motion induced by an oscillating current.

Tanguy, J. C. and Le Goff, M., 2004, **Distortion of the geomagnetic field in volcanic terrains: an experimental study of the Mount Etna stratovolcano**: *Physics of the Earth and Planetary Interiors, v.141*, no.1, p.59-70.
The orientation and intensity of the geomagnetic field were measured on Mount Etna in 1989-1991 at a dozen sites previously sampled for archeomagnetic studies, to determine the variations of these parameters, and possible effects on the archeomagnetic record of volcanic rocks. The averaged values are very close to those measured in sedimentary terrain away from the volcano and with the interpolated IGRF in eastern Sicily, demonstrating that reliable archeomagnetic results can be obtained from volcanic rocks, provided that lavas of the same eruption are sampled on several sites distributed over the largest possible area.

Yu, Y. and Dunlop, D. J., 2003, **Decay-rate dependence of anhysteretic remanence: fundamental origin and paleomagnetic applications**: *Journal of Geophysical Research, v.108*, no.B12, p.1-10.
We measured the intensity of anhysteretic remanent magnetization (ARM) as a function of alternating field (AF) decay rate. For SD and PSD magnetites, ARM increases with decreasing decay rate. MD magnetites have the opposite response. Thermal-activation-theory predicted increases are in reasonable accord with the observed increases for SD material. For MD grains, we hypothesize that increased exposure time (slower decay) permits more efficient self-demagnetization, reducing ARM.

Mineral & Rock Magnetism

Hounslow, M. W. and Morton, A. C., 2004, **Evaluation of sediment provenance using magnetic mineral inclusions in clastic silicates: comparison with heavy mineral analysis**: *Sedimentary Geology, v.171*, no.1-4, p.13-36.
Using recent sediments, transported from known rock sources, it is demonstrated, using discriminant function analysis, that the magnetic properties of the Fe-oxide inclusions provide a clear distinction of primary provenance. It is shown that provenance differences, clearly expressed by the results of heavy mineral analysis, are also sensitively displayed by the magnetic mineral inclusion data. Simple statistical tools are developed to determine a least-noisy subset of magnetic parameters, which are most suitable for stratigraphic provenance discrimination.

Maher, B. A., Karloukovski, V. V. and Mutch, T. J., 2004, **High-field remanence properties of synthetic and natural submicrometre haematites and goethites: significance for environmental contexts**: *Earth & Planetary Science Letters, v.226*, no.3-4, p.491-505.
We identify two high-field parameters which may be of value in identifying and characterizing the high-coercivity components of natural environmental samples. H% indicates the proportion of the room temperature (RT) remanence acquired in fields from 2 T up to 7 T and H_{cool}% indicates the increase or decrease in high-field remanence upon cooling in zero field to 77 K (LT). These parameters can differentiate between goethite-dominated, and haematite-dominated samples.

McEnroe, S. A., *et al.*, 2004, **What is magnetic in the lower crust?**: *Earth & Planetary Science Letters, v.226*, no.1-2, p.175-192.
Long-wavelength and satellite magnetic anomalies require that some regions of the Earth's crust contain minerals that are magnetic at lower crustal conditions. Recent investigations have described hematite-ilmenite magnetism in terms of a new ferrimagnetic substructure, "lamellar magnetism". To look at behaviour of lamellae at mid-to-lower crustal conditions, we studied a Ilm 84 sample. In experiments at 10 kbar as an analog for lower crustal conditions, exsolution lamellae coarsened. If these features were reproduced in the lower crust, hemo-ilmenite or ilmeno-hematite would retain a magnetic moment and high coercivity.

McEnroe, S. A., *et al.*, 2004, **Magnetic anomalies, layered intrusions and Mars**: *Geophysical Research Letters, v.31*, no.19, p.19601.
Studies of remanence-controlled magnetic anomalies on Earth provide possibilities to interpret the nature of the large remanent anomalies on Mars. Such an anomaly, in the Bjerkreim-Sokndal (BKS) Intrusion, shows a minimum of -13000 nT. Modeling of the anomaly requires a natural remanent magnetization (NRM) value of 24 A/m, similar to values invoked to explain Martian anomalies. Magnetic assessment considers hemo-ilmenite, magnetite, and oxide exsolution in clino- and orthopyroxene, and high-temperature ductilely induced lattice-preferred orientation.

Mineral Physics & Chemistry

Faivre, D., *et al.*, 2004, **Mineralogical and isotopic properties of inorganic nanocrystalline magnetites**: *Geochimica et Cosmochimica Acta, v.68*, no.21, p.4395-4403.
Inorganic magnetite nanocrystals were synthesized in an aqueous medium. The nature and morphology of particles were studied by transmission electron microscopy and electron energy loss spectroscopy. At high iron concentrations, euhedral single crystals of pure magnetite with an average characteristic size of 10 nm were formed. Thus low-temperature inorganic processes can lead to the formation of well-crystallized magnetite crystals with narrow size distribution. Oxygen isotope fractionation between magnetite and water was of 0-1‰, similar to that for bacterially produced magnetite.

Gee, S. H., *et al.*, 2004, **Spin orientation of hematite (α-Fe_2O_3) Nanoparticies during the Morin transition**: *IEEE Transactions on Magnetics, v.40*, no.4 Part 2, p.2691-2693.
We have synthesized 40-nm-sized hematite particles to investigate the Morin transition. Mossbauer spectra were obtained from 4.3 to 300 K. The Morin temperature (T-M) was found to be 220 K, lower than 263 K of bulk hematite. Fe^{3+} spins in the 40-nm-sized hematite particle flip from 90° to 28° with respect to the c-axis during the Morin transition, the [110] direction of rhombohedral structure, not in agreement with the 90° to 0° flip observed in bulk hematite or sub- and micron-sized particles.

Sun, W. D., Arculus, R. J., Kamenetsky, V. S. and Binns, R. A., 2004, **Release of gold-bearing fluids in convergent margin magmas prompted by magnetite crystallization**: *Nature, v.431*, no.7011, p.975-978.
A relationship between convergent margin magmas and copper gold ore mineralization has long been recognized(1-6). The nature of the genetic link is controversial. For subduction-related volcanic glasses from the eastern Manus basin, Papua New Guinea, we report decreases in gold and copper abundances, coupled with a switch in the behaviour of titanium and iron as SiO2 rises. We propose that the abrupt depletion in gold and copper results from concurrent sulphur reduction. The subsequent migration and cooling of exsolved aqueous fluids create links between copper-gold mineralization and arc magmatism.

Shvets, I. V., *et al.*, 2004, **Long-range charge order on the Fe_3O_4(001) surface**: *Physical Review B, v.70*, no.15, p.155406-1.
In spite of being the subject of many studies over the last century, the Verwey transition's nature is not fully understood, especially in the case of the magnetite surface. We have atomically resolved the (square root 2* square root 2)R45 degrees reconstructed surface and modeled the results by density functional theory calculations. We attribute the observed pattern to the charge ordering of Fe^{2+}-Fe^{2+} and Fe^{3+}-Fe^{3+} dimers. We propose a mechanism and an explanation for the increase in Verwey transition temperature at surface of magnetite.

Subias, G., *et al.*, 2004, **Magnetite, a model system for mixed-valence oxides, does not show charge ordering**: *Physical Review Letters, v.93*, no.15, p.1-4.
A new set of half-integer and mixed-integer superlattice reflections of the low-temperature phase have been studied by x-ray resonant scattering. None of these reflections show features characteristic of charge ordering (CO). We demonstrate the absence of CO along the c axis with the periodicity of either the cubic lattice q=(001) or the doubled cubic lattice q=(001/2). This result suggests that the Verwey transition is caused by strong electron-phonon interaction instead of an electronic ordering on the octahedral Fe atoms.

Modeling and Theory

Beleggia, M., 2004, **A Fourier-space approach for the computation of magnetostatic interactions between arbitrarily shaped particles**: *IEEE Transactions on Magnetics, v.40*, no.4 Part 2, p.2149-2151.
A new formalism to describe the magnetostatic energy associated with particles of arbitrary shape and magnetization state relies on a Fourier space description of the particle shape, which can be used to obtain explicit expressions for the demagnetization tensor field, magnetic field, magnetic induction and magnetostatic energy of a particle for a given magnetization state. Moreover, the interaction energy between particles, located at arbitrary positions in space, which may have different shapes and magnetization states can also be computed.

Muxworthy, A., Heslop, D. and Williams, W., 2004, **Influence of magnetostatic interactions on first-order-reversal-curve (FORC) diagrams: a micromagnetic approach**: *Geophysical Journal International, v.158*, no.3, p.888-897.
Using a 3-D FFT micromagnetic model of assemblages of ideal SD magnetite-like grains, we show that interactions can strongly affect the magnetic behaviour, for example, interacting assemblages of SD grains can display more MD-like FORC diagrams. Associating the FORC diagram with the Preisach diagram, we find that for moderate and weak interacting SD assemblages, the factorization interpretation of the Preisach diagram is correct, and in agreement with recent experimental results.

NRM Carriers and Origins

Kasama, T., *et al.*, 2004, **Effects of nanoscale exsolution in hematite-ilmenite on the acquisition of stable natural remanent magnetization**: *Earth & Planetary Science Letters, v.224*, no.3-4, p.461-475.
Rocks of the Russell Belt, Adirondack Mountains contain titanohematite with ilmenite lamellae, end-member hematite without lamellae and rare magnetite as potential carriers for the NRM. TEM observations and element mapping by EFTEM indicated that very fine ilmenite lamellae with a minimum thickness ~2 nm are abundant between larger ilmenite lamellae a few hundreds of nanometers thick. The ilmenite lamellae and titanohematite hosts share (001) planes, and the lamellae have coherent, sharp structural and compositional interfaces with their hosts. NRM is correlated with the amount of fine exsolution lamellae, consistent with the lamellar magnetism hypothesis

Kodama, K. P. and Dekkers, M. J., 2004, **Magnetic anisotropy as an aid to identifying CRM and DRM in red sedimentary rocks**: *Studia Geophysica et Geodaetica, v.48*, no.4, p.747-766.
ARM was applied in 9 orientations at fields up to 240 mT to measure magnetite fabric; hematite fabric was measured with IRMs applied in 2 T fields followed by 240 mT af demagnetization, and demagnetization at 90°C to remove the goethite contribution. This approach gave geologically interpretable results, suggesting that the hematite and magnetite both carry a DRM. IRMs applied in 13 T fields were used to measure the magnetic fabric of samples with hematite as their only magnetic mineral. The fabrics that resulted were geologically interpretable, showing a strong NW-SE horizontal lineation consistent with AMS fabrics measured in the same samples. These fabrics suggest that the rock's remanence may have been affected by strain and could have originated as a DRM or a CRM.

Synthesis and Properties of Magnetic Materials

Jana, N. R., Chen, Y. F. and Peng, X. G., 2004, **Size- and shape-controlled magnetic (Cr, Mn, Fe, Co, Ni) oxide nanocrystals via a simple and general approach**: *Chemistry of Materials, v.16*, no.20, p.3931-3935.
A general, reproducible, and simple strategy using generic chemicals is introduced for controlling the size, shape, and size distribution of oxide nanocrystals. The reaction system is generally composed of the metal fatty acid salts, the corresponding fatty acids, and a hydrocarbon solvent. Synthesis of nearly monodisperse Fe_3O_4 nanocrystals in a large size range (3-50 nm) was developed as a model system. The size and shape control of the nanocrystals were achieved by varying the reactivity and concentration of the precursors.

Watanabe, K., Takemura, Y., Shimazu, Y. and Shirakashi, J., 2004, **Magnetic nanostructures fabricated by the atomic force microscopy nano-lithography technique**: *Nanotechnology, v.15*, no.10 Special Issue SI, p.S566-S569.
A local oxidation technique using AFM was performed in order to modify magnetic domain structures in ferromagnetic nanostructures. Co-based nanostructures with a rectangular shape were fabricated by using electron beam lithography followed by AFM nano-oxidation.

Zysler, R. D., Mansilla, M. V. and Fiorani, D., 2004, **Surface effects in α -Fe_2O_3 nanoparticles**: *European Physical Journal B, v.41*, no.2, p.171-175.
The magnetic properties of 5 nm α-Fe_2O_3 nanoparticles have been investigated by magnetization measurements on a sample consisting of homogeneously dispersed, non-interacting, nanoparticles in a polymer matrix. The results indicate that the magnetic properties are mainly determined by surface effects, which manifest themselves in high coercive field, high irreversibility field and shifted hysteresis loop, after field cooling. These effects come from surface anisotropy and exchange anisotropy, due to the coupling between the disordered surface magnetic structure, with multiple spin configurations, and the core antiferromagnetically ordered structure.

…tuffs
continued from p. 1

(We note that one of the tuffs that underlie the Tiva Canyon is the Yucca Mountain Tuff, a name that has been incorrectly applied in the recent rock-magnetic literature to the bootleg samples of the Tiva Canyon Tuff. Although it is too late to eradicate the error, we urge the use of proper stratigraphic nomenclature [Sawyer, et al., 1994] in future publications.)

Devitrification and Crystal Growth

The process of crystal formation here was very similar to that involved in making glass-ceramic synthetic materials [*Worm & Markert*, 1987; *McMillan*, 1979]. Glass forms when liquid compounds with certain chemical compositions cool so quickly that crystals are unable to nucleate and grow. Below the equilibrium melting temperature, the ordered crystalline solid state has a lower free energy than the disordered liquid state, and hence the melt "wants" to crystallize. However there are interfacial energy barriers that must be surmounted in order to effect the transition, and consequently the rates of both nucleation and growth follow Arrhenius-type kinetic laws, i.e., rate is proportional to $\exp(-E_a/kT)$, where E_a is the activation energy, k is Boltzmann's constant and T is absolute temperature.

During cooling, crystals nucleate and grow in each successive temperature interval, to an extent governed by the temperature-dependent rates of those processes and by the time available. It is significant that peak nucleation rates typically occur at temperatures lower than those where crystal growth rates are maximized. Thus slow cooling generally results in nucleation of small numbers of grains that grow to large sizes; conversely more rapid cooling yields finer average grain sizes. When cooling is extremely rapid, as for the quenched rims of submarine basalts, or for small drops of volcanic magma erupted into the atmosphere, there is insufficient time for nucleation and growth to occur before the rates drop to negligible levels at low temperature, and the result is glass, which can be considered a very-high-viscosity metastable liquid or a noncrystalline solid.

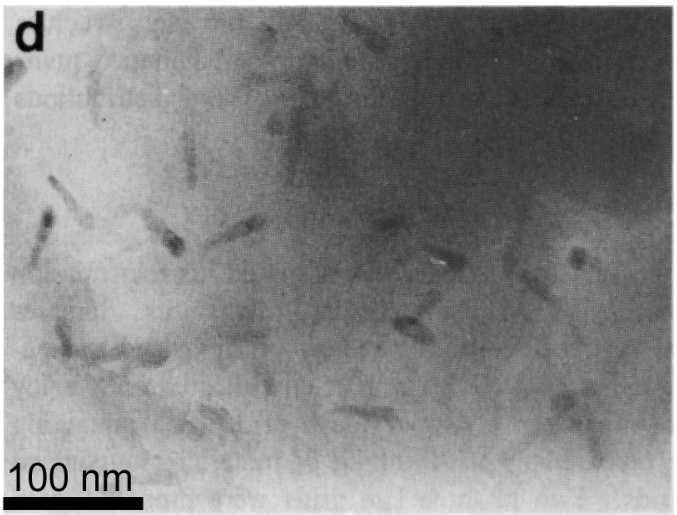

Bright-field TEM image of Fe-Ti oxide nanocrystals in glass in Tiva Canyon Tuff sample CS914 [Schlinger et al., 1991]; average particle dimensions are 50x8.5 nm.

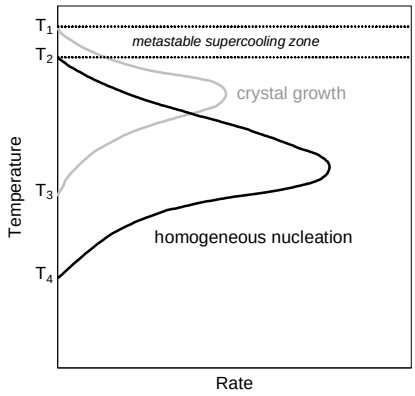

Cooling through the equlibrium melting/ crystallization temperature T_1, a melt of an appropriate composition supercools without crystal formation (unless it is "seeded" or provided with nuclei from an external source). Below T_2 crystals nucleate spontaneously and grow rapidly. Thermal activation and crystal growth rates then progressively diminish at lower temperatures. Peak nucleation rates occur at lower temperatures than peak growth rates. (schematic; redrawn after McMillan, 1979).

Glass-ceramic materials, with various interesting and useful properties, are made by reheating of glass. There is a temperature interval (between T_4 and T_3 in the figure) in which homogeneous nucleation occurs at substantial rates, but growth is negligible. This in essence plants the seeds for growth at higher temperatures of a population of uniformly dispersed, uniformly-sized crystals.

2004 Sampling

This summer we resampled the basal Tiva Canyon section exposed on the west flank of Yucca Mountain, in the same locality previously sampled by *Rosenbaum et al* [1991] and within the sampling area of *Schlinger et al* [1991]. This portion of the unit is rhyolitic in composition, and in addition to vitric material it contains some lithic fragments and pumice lapilli. Surviving holes from previous sampling provided a framework for targeting new sites, and a hand-held "miniKappa"susceptibility meter was used to pinpoint the maximum susceptibility horizon. Samples were collected mainly by drilling, in order to maximize stratigraphic control. A large number of cores were collected from the susceptibility peak for distribution to labs worldwide, and small numbers of additional samples were also collected at sites spanning the lower 10 meters of the Tiva Canyon unit.

After detailed measurements on a representative subset of core specimens at the IRM, we decided to crush and homogenize the samples before distribution, because significant variations in properties were evident, and clearly correlated with varying proportions of pumice and lithic fragments. Samples were first put through a Braun "Chipmunk Crusher", then a rotary disc mill, and finally they were ball milled to produce a fine homogeneous powder. Magnetic properties were remeasured after each step to ensure that no changes had been caused by the processing.

Magnetic Characterization

AC susceptibility and its temperature- and frequency-dependence provide extremely sensitive and diagnostic means of characterizing magnetic nanocrystals. The room-temperature susceptibility of the uncrushed samples rises linearly with height above the base to a sharp maximum and thereafter decays quasi-exponentially. Frequency dependence near the peak generally ranges between about 15% and 30% (see figure below).

Variable-temperature measurements (next page, top) show a more complete picture of the magnetization kinetics. With sufficiently high temperatures and/ or small particle sizes (e.g. 12-03 at room temperature), magnetization remains in equilibrium with the

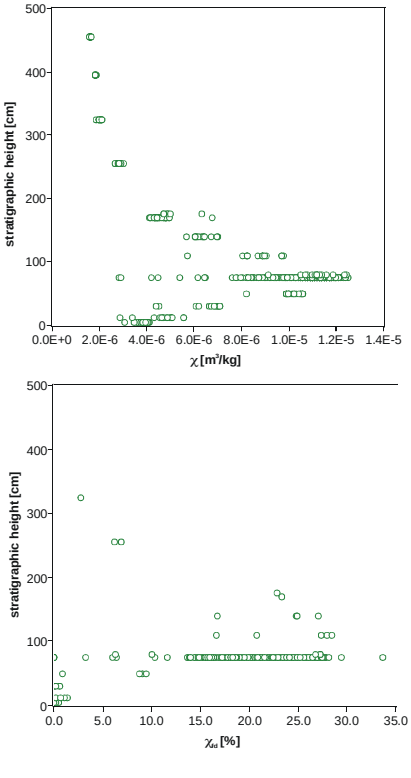

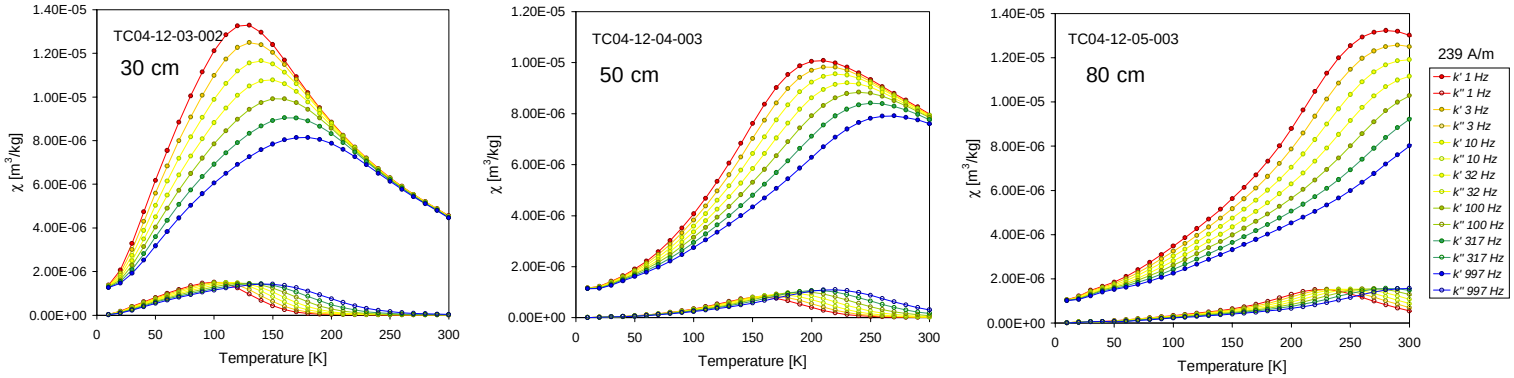

oscillating field at all frequencies: uniaxial particles reverse their polarity in synch with the field, helped by thermal fluctuations to cross the energy barrier between the two polarity states. With decreasing temperature, the equilibrium magnetization increases (and thus so does susceptibility) as thermal randomization diminishes.

Eventually we reach a point where the thermally-activated magnetization kinetics become slow in relation to the ac field reversal rate, and susceptibility drops below the equilibrium value, first for the highest frequency and then for progressively lower frequencies with decreasing temperature. The strongly frequency-dependent "viscous" state is analogous to the strain-rate-dependent rheology of viscous fluids. At the lowest temperatures, the rate of moment reversals becomes negligible, and the assemblage is "blocked in" to a stable single-domain state, analogous to an elastic solid, where susceptibility is due solely to small reversible rotations of grain moments toward the applied field direction.

In Néel's Arrhenius-type rate equation for magnetic moment reversals (in an idealized assemblage of identical noninteracting uniaxial single-domain grains), the activation energy (in small applied fields) is proportional to VM_sH_k: the product of grain volume, saturation magnetization and microscopic coercivity. In a monomineralic assemblage of real particles, $M_s(T)$ is the same for all grains but V and H_k are distributed in some fashion. An elegant but rarely-used method of characterizing the joint $f(V,H_k)$ distribution was developed by *Dunlop* [1965] (see also *Dunlop & Ozdemir* [1997], Figs 8.17 and 17.4), and takes advantage of the fact that application of a strong field H ($<H_k$) decreases the activation energy (for rotation into alignment with the field) in proportion to $(1-H/H_k)^2$.

Dunlop's method begins with application of a weak-field partial thermoremanent magnetization (pTRM) in a temperature interval ($T_1>T_2$), which selectively magnetizes a fraction of grains with activation energies within a narrow range. On a Néel plot (right) this corresponds to grains with (V, H_k) lying between the two low-field blocking contours for T_1 and T_2. Subsequent AF demagnetization progressively erases the pTRM by shifting the room-temperature zero-field blocking contour toward the right in the diagram, and each demagnetization step quantifies the remanence carried by grains in a defined region of the plot, bounded by two low-field, high-temperature and two high-field, room-temperature contours. The whole distribution can be worked out by AF demagnetization of a set of pTRMs covering different temperature intervals.

The reason that this elegant method is not widely used in rock magnetism is of course the rarity of natural materials dominated by noninteracting single-domain grain populations. However the Tiva Canyon samples are excellent for trying it out. There's a twist, though, for the finer-grained samples that are superparamagnetic at room temperature. Because we lack the instruments required to AF demagnetize at low temperature, we have worked out a different method based on the same ideas, using backfield remanence measurements between 10K and room temperature. This is a bit more complicated because, unlike a selective pTRM, the initial saturation remanence at each temperature magnetizes the whole thermally-stable assemblage at that temperature, and rather than erasing the remanence by AF demagnetization, we replace it with another remanence.

In the back-field spectra (derivatives of the backfield remanence curves) each point represents the remanence change associated with a particular temperature and field. Those conditions define a particular blocking contour on the Néel plot, and the corresponding remanence change represents a line integral of the $f(V,H_k)$ distribution along that contour. The problem of reconstructing the entire distribution from a set of backfield measurements is therefore closely related to tomography, which involves reconstruction of a 2- or 3-dimensional function from line integral samples through it. (For example, a measured travel time for a seismic wave represents the line integral of slowness, or reciprocal velocity, along the ray path).

A set of back-field spectra and the calculated $f(V,H_k)$ distribution are shown on the next page for a sample from the maximum-susceptibility layer. With increasing temperature the spectra first shift to lower field values while retaining the same shape and intensity, as the "thermal fluctuation field" grows. Significant unblocking begins above about 150K, where quadrature susceptibility also increases sharply. There is a small spectral component that remains stable above 300K, probably representing the remanence carriers in lithic fragments.

The calculated $f(V,H_k)$ distribution is sharply peaked, with a mode around 3×10^{-24} m^3 and 120 mT. There is a slight streaking towards larger volumes and a very small secondary peak near 10^{-23} m^3, which may be due to the minor ferrimagnetic content of the lithic fragments, or may be a processing artifact.

Assuming that H_k is governed primarily by shape anisotropy, we can approximately calculate the modal aspect ratio from $H_k=\Delta N M_s/2$, using the ellipsoidal formulas for demagnetizing factor N and a value of 420 kA/m for Ms(0K), appropriate for TM10. For this sample, we get L/W~7.5 (L=56 nm, W=7.5 nm), which is in excellent agreement with the dimensions observed by TEM [*Schlinger et al.*, 1991]. Samples from lower in the section, analyzed in the same way, yield modal

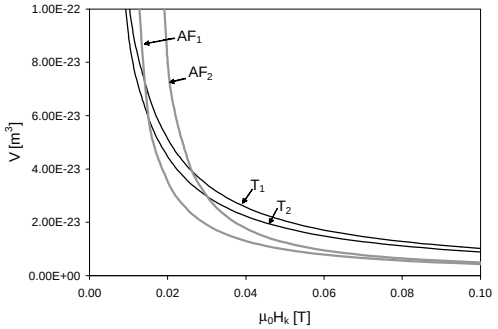

Arrhenius, Svante

b. Feb. 19, 1859, Wijk, Sweden
d. Oct. 2, 1927, Stockholm

An infant prodigy, Arrhenius taught himself to read at age 3. As a doctoral student he made his great discovery that moleclules can break apart into negatively and positively charged ions. This ground breaking work was not at first fully appreciated; his 1884 thesis titled *Recherches sur la conductibilité galvanique des électrolytes* was given the lowest possible passing grade, "not without merit." Eventually the genius of his work was recognized and in 1903 he was awarded the Nobel prize in Chemistry. Also well known is his work on the rate of chemical reactions (Arrhenius Rate equation), and on cosmic physics. Arrhenius also published interesting works on the greenhouse effect and "panspermy", the hypothesis that life on earth originated from spores carried from other planets by radiation.

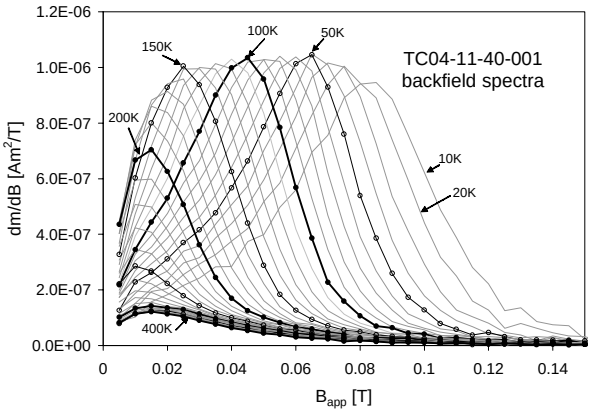

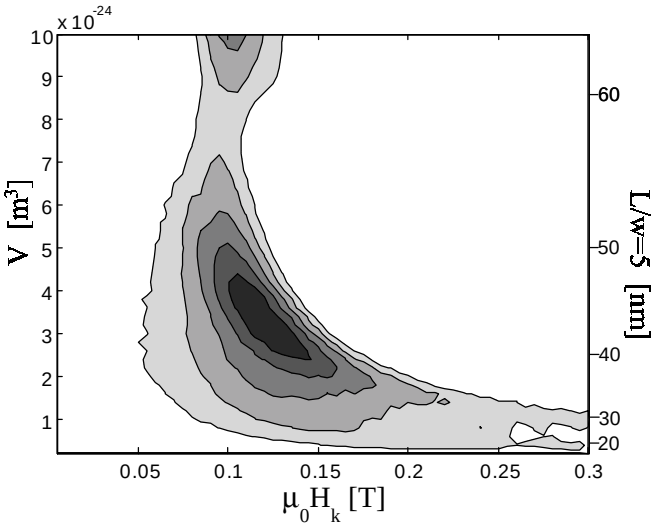

volumes and aspect ratios that show the same trend evident in the TEM images: both decrease toward the base.

In fact there is a very striking and interesting quantitative relationship between grain size and stratigraphic height: on a log plot, there is a nearly perfect straight line, i.e. grain volume or length increase exponentially with stratigraphic height, at least for the first two or three meters. Undoubtedly this is

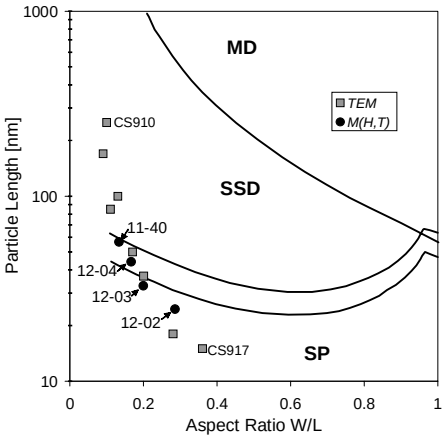

closely related to the Arrhenius kinetics of crystal growth, with exponential dependence on temperature.

Availability

Specimens of the homogenized material are available on request from IRM. In the future (after we finish processing and characterizing the samples) we will also release a set of specimens from higher in the section, with grainsizes primarily in the stable SD range - stay tuned for details.

References

Dunlop, D. J., 1965, Grain distributions in rocks containing single-domain grains: Journal of Geomagnetism and Geoelectricity, v. 17, p. 459–471.

Dunlop, D. J., and Ozdemir, O., 1997, Rock Magnetism: fundamentals and frontiers, Cambridge Studies in Magnetism, Cambridge University Press, 573 p.

Egli, R., and W. Lowrie, Anhysteretic remanent magnetization of fine magnetic particles, *Journal of Geophysical Research-Solid Earth*, *108* (B2), art. no. 2209, 2002.

Eick, P. M. and Schlinger, C. M., 1990, The use of magnetic susceptibility and its frequency dependence for delineation of a magnetic stratigraphy in ash-flow tuffs: Geophysical Research Letters, v.17, no.6, p.783-786.

Pike, C.R., A.P. Roberts, and K.L. Verosub, First-order reversal curve diagrams and thermal relaxation effects in magnetic particles, *Geophysical Journal International*, *145* (3), 721-30, 2001.

Rosenbaum, J. G., 1986, Paleomagnetic directional dispersion produced by plastic deformation in a thick Miocene welded tuff, southern Nevada: implications for welding temperatures: Journal of Geophysical Research B: Solid Earth, v. 91, p. 12,817–12,834.

Rosenbaum, J. G., 1993, Magnetic grain-size variations through an ash-flow sheet: influence on magnetic properties and implications for cooling history: Journal of Geophysical Research B: Solid Earth, v. 98, p. 11,715–11,727.

Rosenbaum, J. G., Hudson, M. R., and Scott, R. B., 1991, Paleomagnetic constraints on the geometry and timing of deformation at Yucca Mountain, Nevada: Journal of Geophysical Research B: Solid Earth, v. 96, p. 1963–1980.

Sawyer, D. A. et al., 1994, Episodic caldera volcanism in the Miocene southwestern Nevada volcanic field; revised stratigraphic framework, $^{40}Ar/^{39}Ar$ geochronology, and implications for magmatism and extension: Geological Society of America Bulletin, v.106, n.10, p.1304-1318.

Schlinger, C. M., Rosenbaum, J. G. and Veblen, D. R., 1988, Fe-oxide microcrystals in welded tuff from southern Nevada; origin of remanence carriers by precipitation in volcanic glass: Geology, v.16, no.6, p.556-559.

Schlinger, C. M., Veblen, D. R., and Rosenbaum, J. G., 1991, Magnetism and magnetic mineralogy of ash flow tuffs from Yucca Mountain, Nevada: Journal of Geophysical Research B: Solid Earth, v. 96, p. 6035–6052.

Worm, H.-U., and Markert, H., 1987, The preparation of dispersed titanomagnetite particles by the glass-ceramic method: Physics of the Earth and Planetary Interiors, v. 46, p. 263–270.

Worm, H.-U., and Jackson, M., 1999, The superparamagnetism of Yucca Mountain Tuff: Journal of Geophysical Research B: Solid Earth, v. 104, no. B11, p. 25,415-25,425.

Worm, H.-U., and Jackson, M., 2000, Magnetic viscosity of Yucca Mountain Tuff: Ideal single-domain behavior: EGS 25th General Assembly.

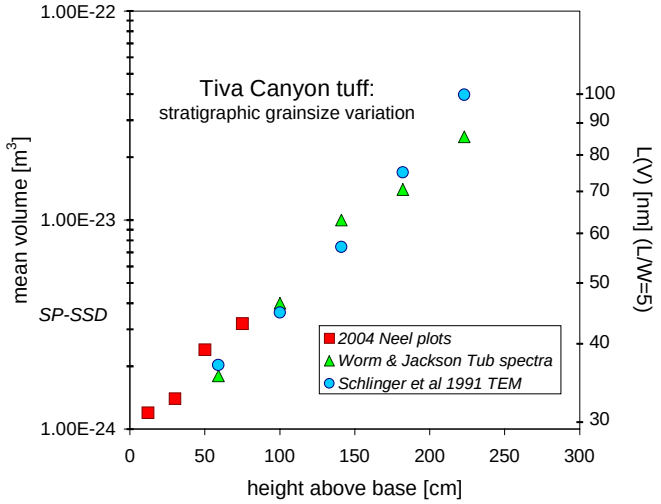

The *Institute for Rock Magnetism* is dedicated to providing state-of-the-art facilities and technical expertise free of charge to any interested researcher who applies and is accepted as a Visiting Fellow. Short proposals are accepted semi-annually in spring and fall for work to be done in a 10-day period during the following half year. Shorter, less formal visits are arranged on an individual basis through the Facilities Manager.

The *IRM* staff consists of **Subir Banerjee**, Professor/Director; **Bruce Moskowitz**, Professor/Associate Director; **Jim Marvin**, Emeritus Scientist; **Mike Jackson**, **Peat Sølheid**, and **Brian Carter-Stiglitz**, Staff Scientists.

Funding for the *IRM* is provided by the **National Science Foundation**, the **W. M. Keck Foundation**, and the **University of Minnesota**.

The *IRM Quarterly* is published four times a year by the staff of the *IRM*. If you or someone you know would like to be on our mailing list, if you have something you would like to contribute (*e.g.*, titles plus abstracts of papers in press), or if you have any suggestions to improve the newsletter, please notify the editor:

Mike Jackson
Institute for Rock Magnetism
University of Minnesota
291 Shepherd Laboratories
100 Union Street S. E.
Minneapolis, MN 55455-0128
phone: (612) 624-5274
fax: (612) 625-7502
e-mail: irm@umn.edu
www.irm.edu

IRM

UNIVERSITY OF MINNESOTA

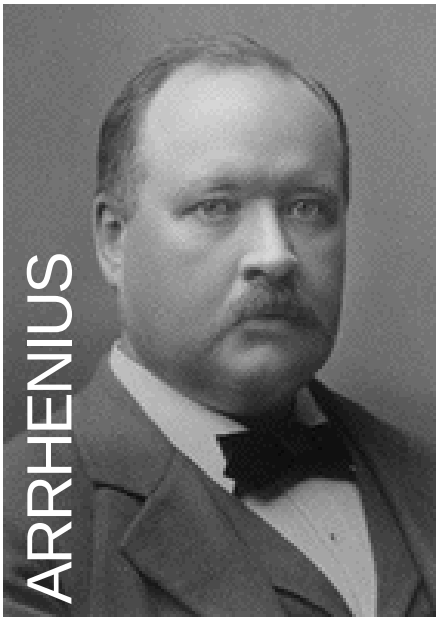

http://nobelprize.org/chemistry/laureates/1903/arrhenius.jpg

Collector's Series #35

The IRM Quarterly

University of Minnesota
291 Shepherd Laboratories
100 Union Street S. E.
Minneapolis, MN 55455-0128
phone: (612) 624-5274
fax: (612) 625-7502
e-mail: irm@umn.edu
http://www.irm.umn.edu/

Nonprofit Org.
U.S Postage
PAID
Mpls., MN
Permit No. 155